Acoustic Emission Enabled Particle Size Estimation via Low Stress-Varied Axial Interface Shearing

Min Yu, *Member, IEEE*, Tom Reddyhoff, Daniele Dini, Andrew Holmes, *Member, IEEE*, and Catherine O'Sullivan

***Abstract*— Acoustic emission (AE) refers to a rapid release of localized stress energy that propagates as a transient elastic wave and is typically used in geotechnical applications to study stick-slip during shearing, and breakage and fracture of particles. This article develops a novel method of estimating the particle size, an important characteristic of granular materials, using axial interface shearing-induced AE signals. Specifically, a test setup that enables axial interface shearing between a 1-D compression granular deposit and a smooth shaft surface is developed. The interface sliding speed (up to 3 mm/s), the compression stress (0–135 kPa), and the particle size (150 μm–5 mm) are varied to test the acoustic response. The start and end moments of a shearing motion, between which a burst of AE data are produced, are identified through the variation of the AE count rates before key parameters can be extracted from the bursts of interests. Linear regression models are then built to correlate the AE parameters with particle size, where a comprehensive evaluation and comparison in terms of estimation errors is performed. For granular samples with a single size, it is found that both the AE energy-related parameters and AE counts, obtained using an appropriate threshold voltage, are effective in differentiating the particle size, exhibiting low fitting errors. The value of this technique lies in its potential application to field testing, for example, as an add-on to cone penetration test systems and to enable *in situ* characterization of geological deposits.**

***Index Terms*— Acoustic emission (AE), interface shear, linear regression, particle size, signal processing.**

I. Introduction

ACOUSTIC emission (AE) is a phenomenon of a rapid release of localized stress energy caused by friction [1], impact [2], [3], cavitation, etc. Once released, this energy propagates as a transient elastic wave through materials and structures and it can be recorded using appropriate instrumentation. The AE technique has been widely employed to: 1) determine the locations where the event leading to the energy release occurred; 2) characterization of the mechanical properties of materials/structures; and 3) structural health monitoring, for example, crack growth in a pressure container, and variation of friction in dry and lubricated contacts [4]–[8]. Recently, research on the use of AE in engineering applications has focused on advanced signal processing methods such as machine learning-enabled correlation models [9], theoretical modeling and numerical simulation for better understanding of mechanism of AE generation [6], [10], [11].

In geomechanics AE has been used to probe particle breakage and the initiation of failure in rock, in particular, the location of micro-fractures [12], [13]; an AE sensor has been integrated in a multi-sensing cone penetrometer, together with strain gauges (for penetration resistive and shearing force measurements), dielectric sensors (for soil moisture detection), and near-infrared sensors, leading to a possibility of information fusion and thus a more accurate prediction of soil properties [14], [15]. In laboratory testing correlations between the AE parameters of counts and count rates and the stress–strain characteristics in a tri-axial compression test have been explored [16]; AE counts and energy have correlated with soil deformation regimes and void ratios during a confined uniaxial compression of soil samples [17]; the AE technique has been also employed to detect stick-slip failure [18], [19] and the variation of the stress chains [20] in sheared granular materials, enabling remote monitoring of the state of granular layers in earthquake systems.

This article aims to establish how the particle size, an important characteristic of granular materials, can be inferred using axial interface shearing-induced AE signals. This technique is of value to field testing applications such as the cone penetration test and new types of robots that may be deployed in site investigation. It contrasts with in-lab measurements of the particle size, which have been used for decades [21]–[23]. Other existing work that advances in field soil classification function is using shearing-induced friction of a cone penetrometer, as coupled with the measurements of tip resistance and pore pressure, to estimate the particle size of the soil nearby [24]. In particular, the cone penetrometer has been modified with textured surfaces in a diamond pattern to enhance the friction sensitivity to the interface shearing (this method is achieved based on a large amount of previous in-lab investigation [25]–[27], for example, the influence of the surface roughness on shearing characteristics.

Manuscript received December 16, 2021; revised February 13, 2022; accepted February 26, 2022. Date of publication March 2, 2022; date of current version March 16, 2022. This work was supported by the Natural Environment Research Council (NERC) under Grant NE/T010983/1. *(Corresponding author: Min Yu.)*

Min Yu, Tom Reddyhoff, and Daniele Dini are with the Department of Mechanical Engineering, Imperial College London, London SW7 2AZ, U.K. (e-mail: m.yu14@imperial.ac.uk; t.reddyhoff@imperial.ac.uk; d.dini@imperial.ac.uk).

Andrew Holmes is with the Department of Electrical and Electronic Engineering, Imperial College London, London SW7 2AZ, U.K. (e-mail: a.holmes@imperial.ac.uk).

Catherine O'Sullivan is with the Department of Civil and Environmental Engineering, Imperial College London, London SW7 2AZ, U.K. (e-mail: cath.osullivan@imperial.ac.uk).

Digital Object Identifier 10.1109/TIM.2022.3156175

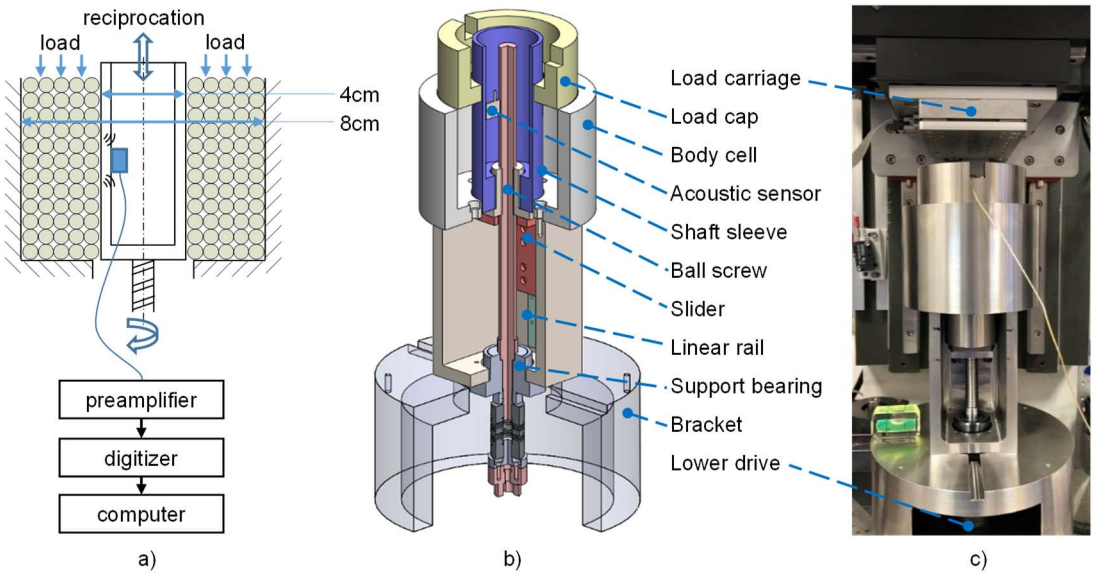

Fig. 1. Test setup of a ball screw driven axial interface shear in a 1-D compressed deposit of glass ballotini. (a) Schematics of the overall system. (b) Isometric section view. (c) Physical implementation.

Other AE-enabled particle size estimation concentrates in the application to pneumatically conveyed pulverized fuel, the size distribution of which is important to combustion process. Specifically, an AE sensor and a metallic waveguide have been integrated into a pneumatic pipe to detect each burst AE signal that is caused by an individual particle impact event, and a theoretical relationship is established based on Hertz contact theory to extract the particle size from the AE peak voltage [28]–[30].

The main contributions of the present work are as follows.

1) A test setup is developed to enable axial interface shearing between a granular deposit subject to 1-D compression and a smooth shaft surface, inside which a piezoelectric sensor is deployed to capture shear-induced AE signals.
2) AE signals are processed to extract key parameters from bursts of data (as produced by intermittent motion of interface shearing), the start and end moments of each burst are identified through the variation of AE count rates.
3) By considering the acoustic response to varied interface sliding speed, compression stress, and particle size, linear regression models are built to correlate different AE parameters with the particle size of granular materials.

II. Test Setup of 1-D Compression and Axial Interface Shear

For in-field geotechnical applications such as in cone penetration testers [14], [24] and new in-site investigation tools of bio-inspired burrowing robots [31], a steel rod with a conical tip (3.6–4.4 cm in the diameter) is commonly adopted as the framework structure of an instrumentation set-up, which moves into the soil from low-stress (near ground) to high-stress area (deeper underground) at a controlled speed. Therefore, to reproduce the cone penetration testing environment, in the present proof work with AE measurements, a test setup is developed to enable stress-varied axial interface shearing of granular particles, adjacent to a motion-controlled shaft sleeve (4 cm in the diameter). A test setup is developed to enable AE measurements of granular particles under low-stress axial interface shearing, adjacent to a motion-controlled shaft sleeve (4 cm in diameter). As shown in Fig. 1(b), a ball screw–linear rail assembly is employed to convert the rotation of a lower drive to reciprocation of the shaft sleeve, and 1-D compression of glass ballotini specimens is achieved with a vertical force being applied by a load carriage. A miniature acoustic sensor (Mistras PICO [32]), which records the sound radiated from the rubbing interface and particles undergoing collision, is attached on the inner surface of the hollow shaft sleeve. The captured AE signals are conditioned by a preamplifier (Mistras 2/4/6 preamplifier [33]), the amplification setting of which is switched at 40 dB with an integrated 20 kHz–2 MHz

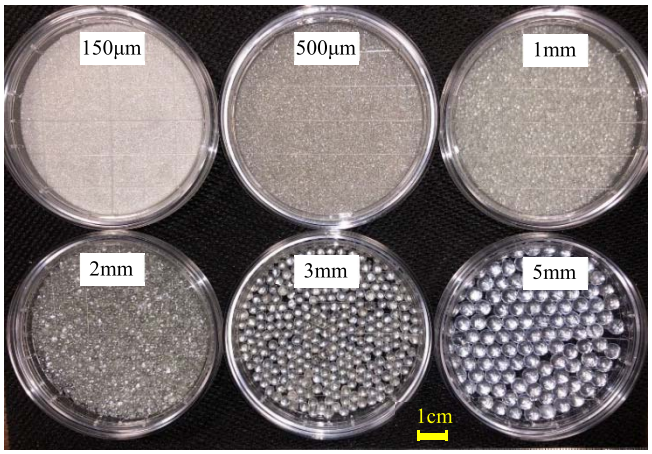

Fig. 2. Test specimens of glass ballotini with the diameters of 150 μm, 500 μm, 1 mm, 2 mm, 3 mm, and 5 mm.

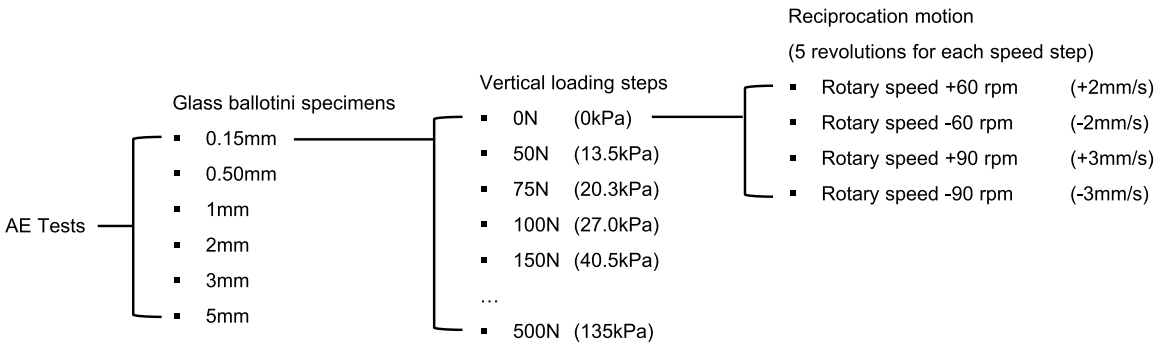

Fig. 3. Test configurations for AE experimental tests of axial interface shear: illustration of variation in sizes of glass ballotini specimens, compression stress, and sliding speed.

TABLE I
PROPERTIES OF GLASS BALLOTINI SPECIMENS IN AE EXPERIMENTAL TESTS

Glass ballotini Size (mm)	Diameter range (mm)	Bulk Density (kg/m^3)	Void Ratio* (-)
0.15	0.1-0.2	1515	0.65
0.5	0.4-0.6	1530	0.63
1	1.0-1.3	1432	0.75
2	1.7-2.1	1472	0.70
3	2.85-3.45	1535	0.63
5	4.70-5.30	1615	0.55

* Void ratios of glass ballotini specimens are estimated as: (1000 kg/m^3 × specific gravity – bulk density) / (bulk density), where the nominal value of specific gravity of glass ballotini is 2.5. Moreover, the void ratios are deemed to be constants in the present study, as the particle deformation during the loading tests is negligible according to the vertical displacement measured by a LVDT sensor.

bandwidth filter, enabling a conversion from a weak electrical signal (in the acoustic sensor end) to an output signal strong enough to be noise-tolerant, before feeding into a digitizer (Mistras PCI-2 [34]) and logged by a computer. The overall design illustrated in Fig. 1(b) is further integrated and implemented in a universal mechanical tester (Bruker UMT [35], [36]), which provides a rotary speed $\omega \in$ [–90 r/min, +90 r/min] (or a linear speed of the sliding shaft sleeve $v \in$ [−3 mm/s, +3 mm/s], given a 2 mm pitch of the ball screw) and a vertical load $F \in$ [0 N, 500 N] (or the equivalent compression stress $\sigma \in$ [0 kPa, 135 kPa]). Fig. 2 shows images of six groups of single-size glass ballotini specimens used in the AE tests, with the particle diameter $D \in$ [150 μm, 5mm] and the mechanical properties listed in Table I. The selection of these specimens is due to that drained and round glass ballotini are often used as a model soil in geomechanical research, with different sizes corresponding to different categories of real soils/sands [16]–[20]. To characterize the influence of the particle size D, the interface sliding speed v, and the compression stress σ on the acoustic response, the parameters considered in the AE experimental tests are varied and detailed in Fig. 3.

III. AE SIGNAL PROCESSING

Note that, in this work, "session," "burst," "interval," and "point" are defined as follows: a test session has a fixed time length of 250 s, during which AE data is logged, and during which intermittent periods of shearing motion occur; a burst of AE data refers to the signal generated by a continuous shearing motion [e.g., there are four bursts of AE data displayed in Fig. 5(a)], the time duration of each burst is between 5–7 s in the case of the present testing profiles; an analysis interval of AE data is constructed using a fixed time duration 0.1 s of data (i.e., 2×10^4 AE data points in each analysis interval), as defined in Fig. 4, and is needed to calculate interval AE parameters, such as interval AE counts and interval AE count rates; an AE data point refers to the sample recorded at the system sampling frequency of 200 kHz, that is, an analysis interval has 2×10^4 AE data points.

A. Parameters Extraction From AE Data

The AE data acquisition system operates at a sampling frequency of 200 kHz, the duration of a single AE test session is fixed at 250 s, as determined by the data logging system, thus producing a total number of 5×10^7 data points per test session. To better extract AE parameters such as AE counts and AE count rates, the original data is divided into a series of "analysis interval of AE data," each with a fixed duration of 0.1 s, which is selected as a compromise between time resolution (of the reconstructed series of AE analysis intervals) and signal noise–a shorter duration (than 0.1 s) leads to more noise in the signal derivate (the signal derivate is needed in the calculation of AE count rates), while a larger time period means poor time resolution (of the reconstructed series of AE analysis intervals). The rearrangement of the AE data, together with the definition of the parameters of interval AE energy, counts, and frequencies, are illustrated in Fig. 4.

Fig. 5(a) shows an example of AE data recorded over a time period of 60 s for a specimen with 1 mm glass ballotini and an applied constant load of 50N (equivalent to 13.5 kPa) and two cycles of reciprocation (at 2 and 3 mm/s, respectively). The time–frequency response with a time resolution of 0.1 s is plotted in Fig. 5(b), from which frequency-related AE parameters can be extracted. Additionally, a histogram of AE noise data collected over a period of 10 s (in the stationary case) is plotted in Fig. 5(c), showing a maximum amplitude of around 15 mV. The AE parameters extracted from additional AE tests with 2, 3, and 5 mm glass ballotini specimens are provided in Fig. 6, including interval AE counts at two different threshold voltages of 0 and 20 mV, interval AE

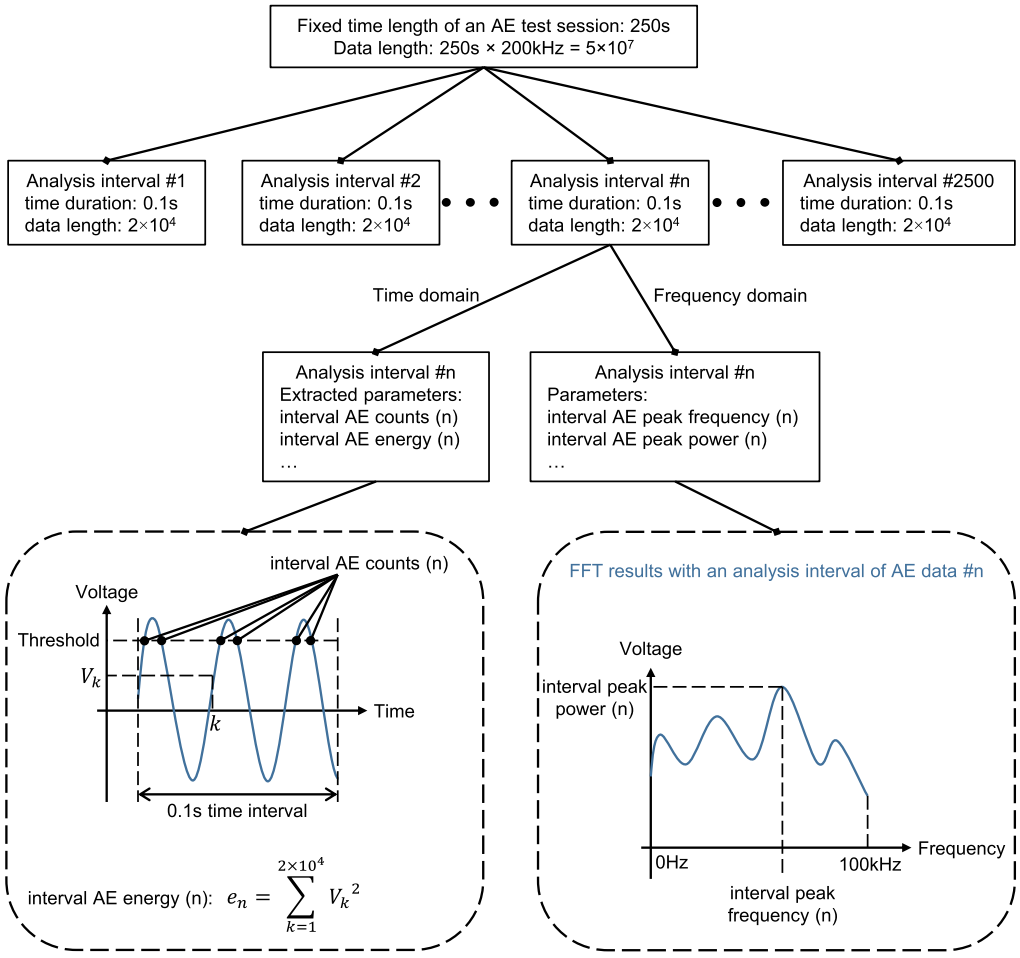

Fig. 4. Procedures used to extract time-domain and frequency-domain parameters from the AE data captured. The energy of the nth analysis interval of AE data (denoted as "interval AE energy") is calculated as $e_n = \sum(V_k^2)$, where V_k is the amplitude of the kth AE data point in the 0.1 s analysis interval (20k points in total).

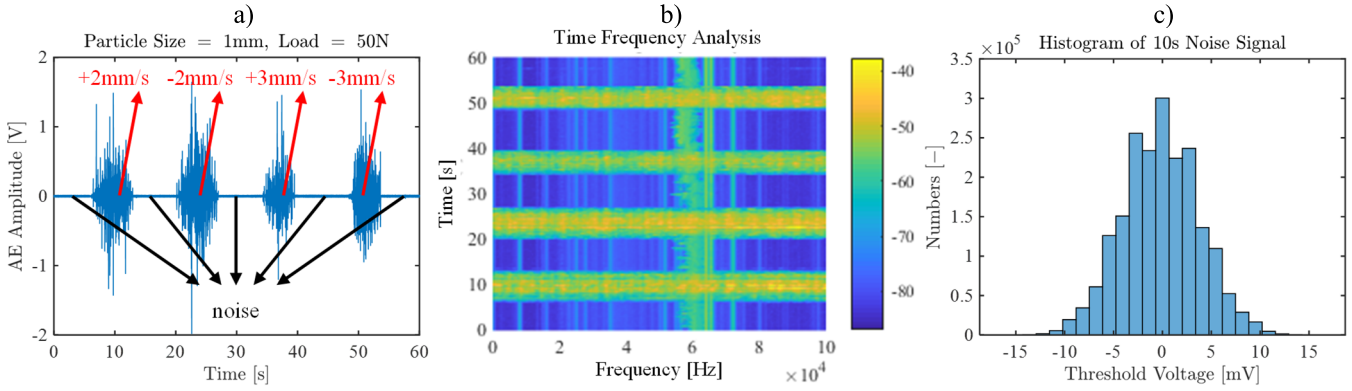

Fig. 5. (a) Example of a time series of original AE data with 1 mm glass ballotini specimens and 50 N constant load (equivalent to 13.5 kPa). (b) Its time–frequency analysis with a time resolution of 0.1 s. (c) Histogram of a 10 s of noise AE data.

count rates (derivatives of interval AE counts), interval AE energy, and interval AE median and mean frequencies, where the time resolution is also 0.1 s (as synchronous with that of data series of AE analysis intervals). The moments of transition between static and sliding friction (i.e., an interface shearing) can be clearly identified using either interval AE count at 0 mV threshold voltage or interval AE count rates (see Fig. 6 (rows 2 and 3), respectively), where a significant change can be seen. This identification helps find the exact data segments of interest (denoted as "bursts of AE data"), enabling subsequent data processing that aims to correlate the shear-induced AE with the particle size, compression stress,

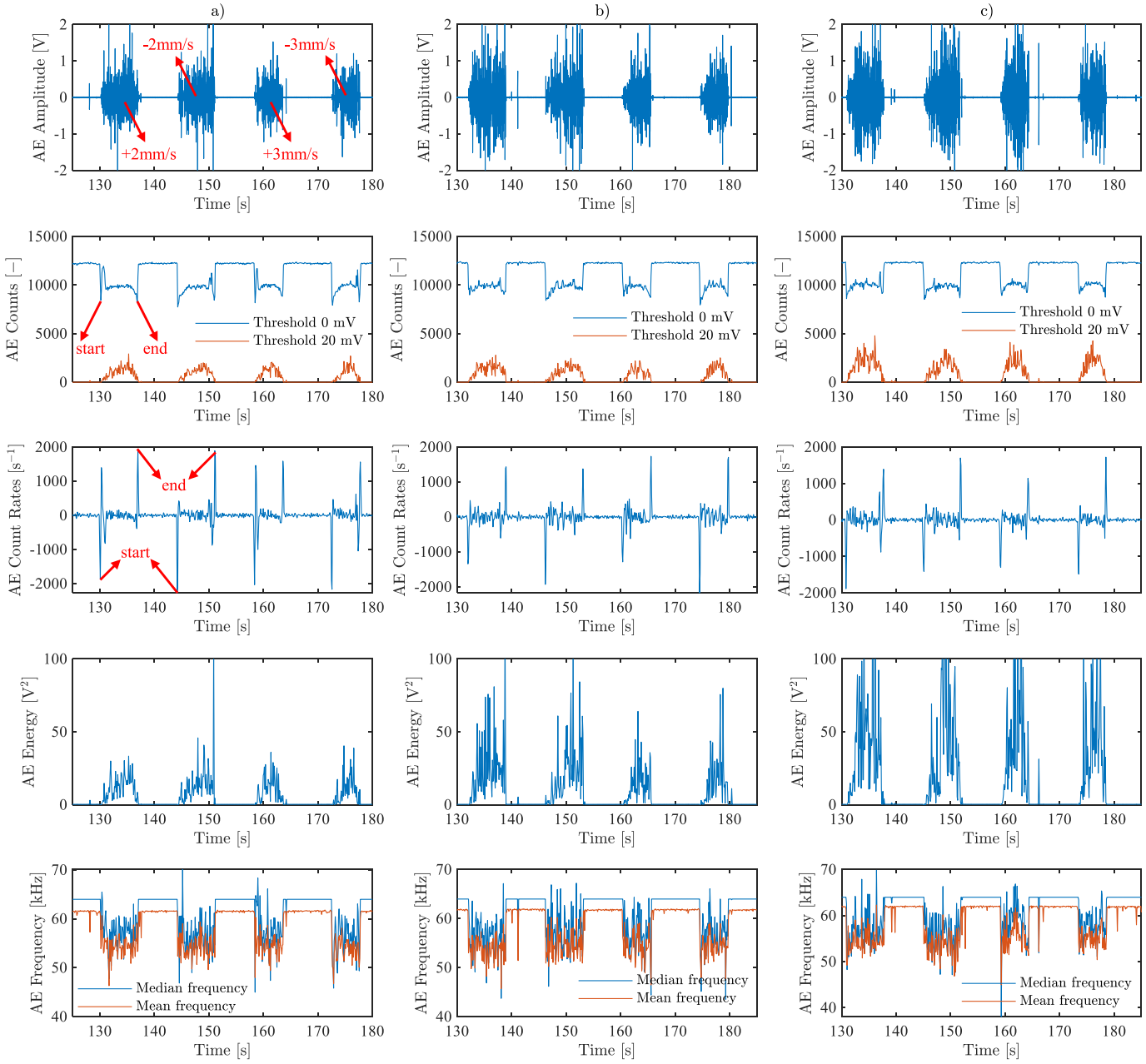

Fig. 6. Extraction of interval AE parameters (a)–(c) example test results with 2, 3, and 5 mm glass ballotini under the same constant load of 75 N (equivalent to 20 kPa). The AE parameters, from the top to bottom rows, are original AE amplitude, interval AE counts at two different threshold voltages of 0 and 20 mV, interval AE count rates (derivatives of interval AE counts), interval AE energy, and interval AE median and mean frequencies (as extracted from time–frequency analysis). The speed "+/– 2 mm/s and +/– 3 mm/s" denotes the sliding speed of the shaft sleeve. The annotations of "start" and "end" correspond to the start and end moments of an axial interface shear motion.

and interface sliding speed (see later in Section III-B). Other representative AE parameters including interval AE energy and interval mean/median frequencies are also provided in Fig. 6 (row 4 and 5), respectively.

B. Correlation Between Particle Size and Burst AE Parameter

To correlate the particle size with the AE parameters extracted from a data burst obtained during an axial interface shear motion (i.e., during a single reciprocation) [see in Fig. 6 (rows 2 and 3)], the burst AE energy $E_{D,\sigma,\upsilon}$ is considered and given as

$$E_{D,\sigma,\upsilon} = \left[\sum_{n=n_s}^{n=n_e} e_n\right] \Big/ (n_e - n_s + 1)$$
$$= \left[\sum_{n=n_s}^{n=n_e} \left(\sum_{k=1}^{2\times 10^4} V_k^2\right)\right] \Big/ (n_e - n_s + 1) \quad (1)$$

where the subscripts D, σ and υ indicate the AE test condition of the diameter of the glass ballotini, the compression stress and the interface sliding speed ($\upsilon = \omega \cdot P$, where $P = 2$ mm is the thread pitch and ω is the rotary speed of the lower

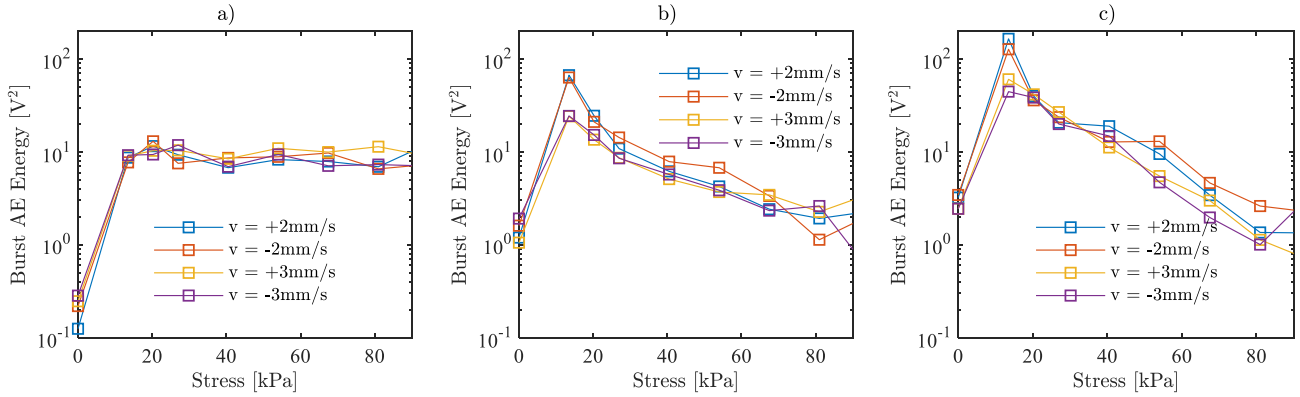

Fig. 7. Effect of interface sliding speed on the AE response (a)–(c) burst AE energy $E_{D,\sigma,v}$ against compression stress σ with the particle size $D = 2$, 3, and 5 mm.

drive), respectively, n is the number of the nth interval AE data (as defined in Fig. 4), n_s and n_e are the start and end numbers of interval AE data respectively, and e_n is the energy of the nth interval AE data (as defined in Fig. 4). This energy is further unified by dividing the time duration (i.e., the total numbers of analysis intervals over a burst of AE data, $n_e - n_s + 1$). Similarly, the burst AE count, denoted $C_{D,\sigma,v}$, is given as

$$C_{D,\sigma,v} = \left[\sum_{n=n_s}^{n=n_e} c_n\right] \Big/ (n_e - n_s + 1) \tag{2}$$

where c_n is the interval AE count.

Fig. 7 shows the burst AE energy $E_{D,\sigma,v}$ against the compression stress σ for glass ballotini specimens with different particle sizes of ($D = 2$, 3, and 5 mm), it can be seen the acoustic response is insensitive to the interface sliding speed. To correlate the particle size and the AE parameters, Fig. 8 depicts and compares burst AE parameters with all six glass ballotini specimens tested ($D = [0.15, 0.5, 1, 2, 3, 5]$ mm), proves that the parameters of the AE counts with 0 mV threshold voltage, and the mean and median frequencies do not clearly systematically vary with the particle size, whereas the AE signal intensity reduces significantly with decreasing particle size [see Fig. 8(a)]. On the other hand, the AE signal intensity increases with increasing stress in the range of $\sigma \in [0\ 20]$ kPa, before decreasing and stabilizing at a lower value. This phenomenon can perhaps be explained by how the sound radiation is generated: in the low compression stress case, the AE is mainly due to shear-induced elastic collision of particles near the interface, in contrast the much stiffer particle deposit under increased compressive stress will substantially inhibit particle collision, thus making the particle-shaft sliding interface the main AE source. It should be noted that, according to the findings in [21], surface texturing of the shaft could be used to promote shearing collisions between particles.

The peak value of the burst AE energy considering all stress levels applied during the load tests, $\max(E_{D,\sigma,v})$, can be selected as the AE parameter that correlates best with the particle size D, exhibiting an almost linear correlation when the AE energy and particle size are both plotted on a logarithmic axis, as shown in Fig. 9(a). Also, the AE counts with threshold voltages no less than 20 mV (i.e., the peak magnitude of AE noise signal as found in Fig. 5(c) can also be correlated with the particle size, with small fitting deviations, as shown in Fig. 9(c) and (d).

To further assess the correlation between the AE signal and the particle size, a group of mixed sizes of glass ballotini specimens (known as "gap-graded granular materials" [37]) are tested by following the same experimental procedures in Fig. 3, including 25% 3 mm + 75% 1 mm, 50% 3 mm + 50% 1 mm, 75% 3 mm + 25% 1 mm, 25% 5 mm + 75% 1 mm, 50% 5 mm + 50% 1 mm, and 75% 5 mm + 25% 1 mm (all percentages refer to the volumetric proportions). The linear regression results are shown in Fig. 10, the dashed lines are the linear models only with the AE data of single size specimens (thus the same ones displayed in Fig. 9), while the solid lines refer to the linear models fit by the AE data of both the single size and the gap-graded particle specimens. Note that the weighted arithmetic mean diameters are used as D in the case of gap-graded grains. Fig. 10(a) shows that the presence of different sizes of glass ballotini attenuates the AE signal intensity as compared to the AE response to the single size specimens, so that these two linear models do not collapse into the same curve. This attenuation could also be determined by: 1) the diameter ratio of the coarse and fine particles and 2) volumetric proportion between them [37]. Despite these complexities, the AE counts at 20 mV threshold voltage can present two linear models that are relatively close to each other, as seen in Fig. 10(b).

To normalize the scales and ranges of the fitting errors of the linear models in Figs. 9 and 10, a normalized root mean square error (NRMSE) is introduced to facilitate reasonable model assessment and comparison. The NRMSE can be interpreted as a fraction of the overall range (in the y-axis) that is typically determined by these linear models, and it is mathematically defined in (3), by taking the case of the AE energy as an example

$$\text{NRMSE} = \frac{\sqrt{\dfrac{\sum_{i=1}^{i=\max(i)}\left[\left(\log_{10}\hat{E}_i - \log_{10}E_i\right)^2\right]}{\max(i)}}}{\max\left(\log_{10}\hat{E}_i\right) - \min\left(\log_{10}\hat{E}_i\right)} \tag{3}$$

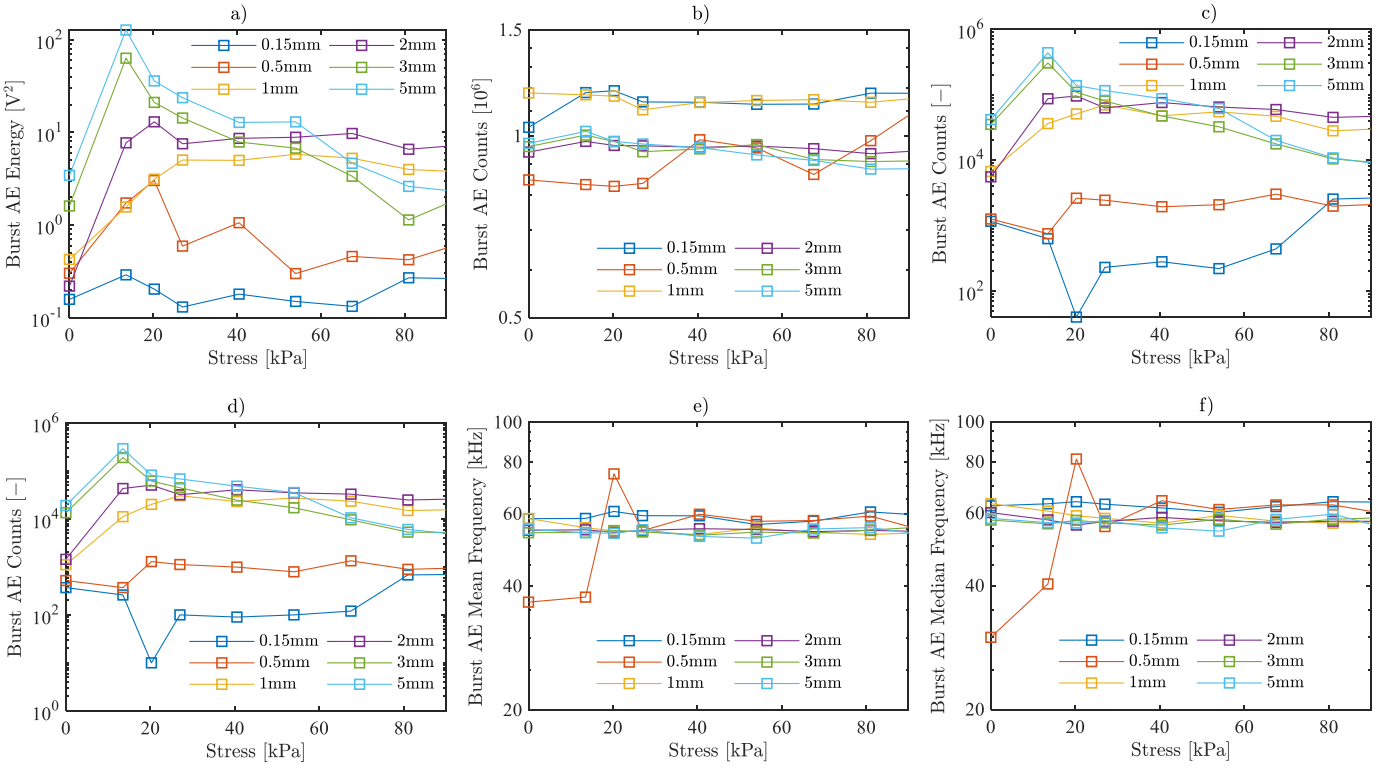

Fig. 8. Different burst AE parameters of (a) burst AE energy $E_{D,\sigma,v}$, (b) burst AE counts (with 0 mV threshold voltage), (c) burst AE counts (with 20 mV threshold voltage), (d) burst AE counts (with 40 mV threshold voltage), (e) burst AE mean frequency, and (f) burst AE mean frequency against the compression stress σ, where the results with a group of glass ballotini specimens (D = [0.15, 0.5, 1, 2, 3, 5] mm) are presented. Note all data here are with the same interface sliding speed of –2 mm/s.

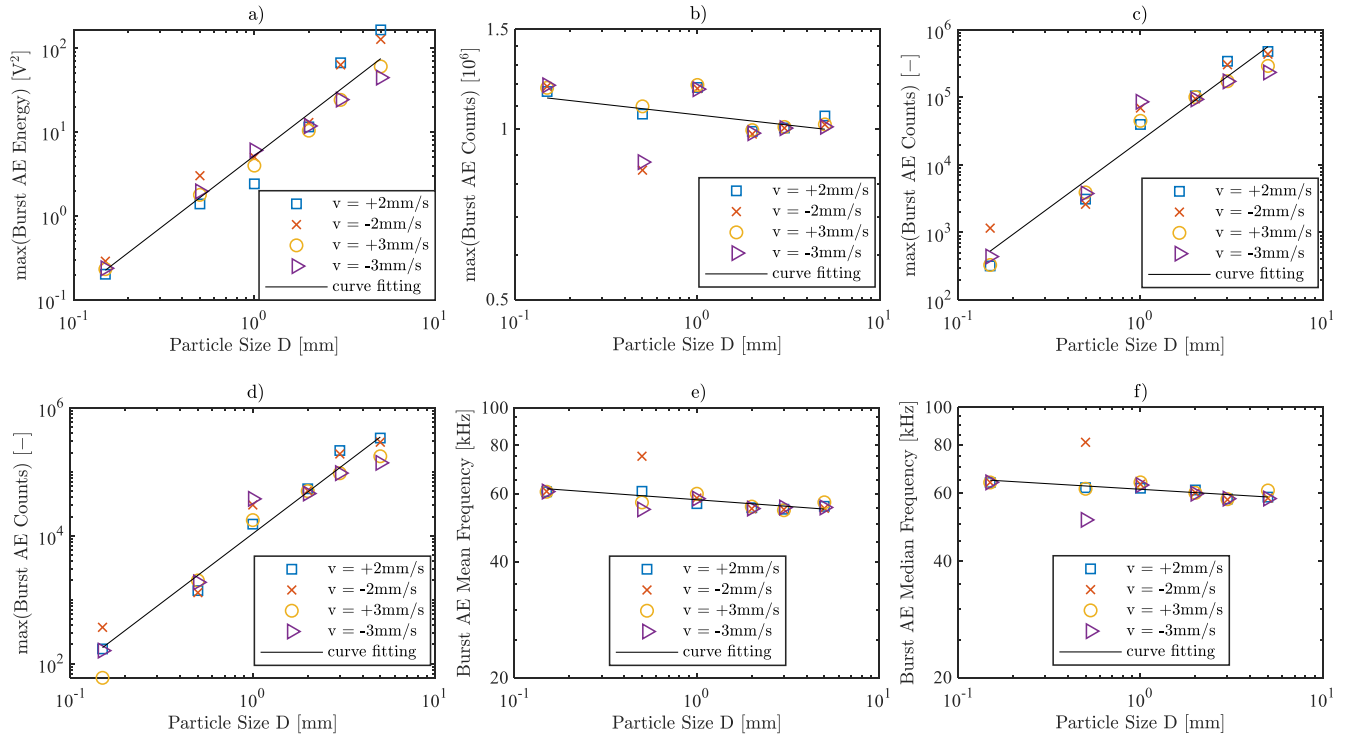

Fig. 9. Linear regression between the particle size D and (a) peak values of burst AE energy, $\max(E_{D,\sigma,v})$, (b) peak values of burst AE counts with 0 mV threshold voltage, (c) peak values of burst AE counts with 20-mV threshold voltage, (d) peak values of the burst AE counts with 40 mV threshold voltage, (e) burst AE mean frequencies, and (f) burst AE median frequencies.

where E_i is the AE energy value used as y-coordinate in Figs. 9(a) and 10(a), $\hat{E}_i$ is the AE energy estimated by the linear model. The NRMSEs for other AE parameters are defined in the same form as (3) and summarized in Fig. 11,

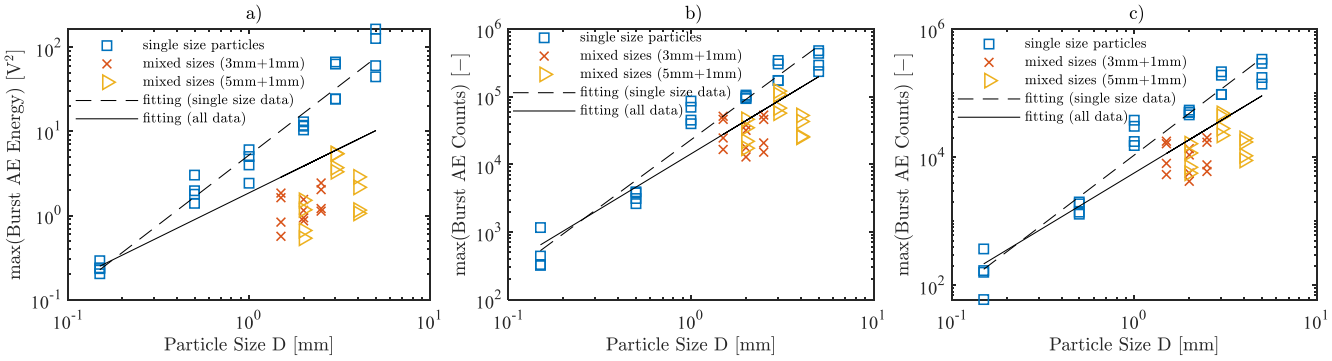

Fig. 10. Linear regression between the particle size D and different AE parameters, where mixed sizes of glass ballotini specimens include 25% 3 mm + 75% 1 mm, 50% 3 mm + 50% 1 mm, and 75% 3 mm + 25% 1 mm, shown as "red cross" from left to right in each plot, and 25% 5 mm + 75% 1 mm, 50% 5 mm + 50% 1 mm, and 75% 5 mm + 25% 1 mm, shown as "yellow triangle" from left to right in each plot. All percentages refer to the volumetric proportions.

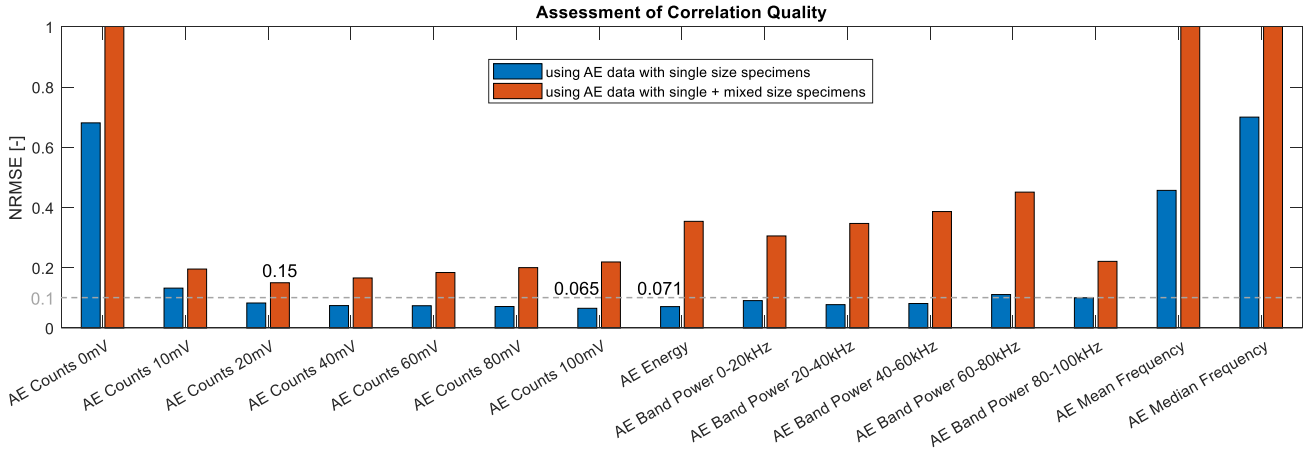

Fig. 11. Fitting errors of the linear regression models between the particle diameter and different AE parameters, as evaluated using NRMSEs defined in (3). Note that NRMSE values greater than 1 are chopped.

where the blue bars refer to NRMSEs only with only the AE data of single size specimens taken into account and the red bars are the cases that both the single and mixed sizes of specimens are dealt.

It can be concluded that AE energy-related parameters (including the AE band power at different frequency bandwidth) and AE counts with threshold voltages between 20 and 100 mV can be used to estimate the particle size–this is probably because the voltage within 20 mV is likely interfered by the AE noise signal [according to the histogram in Fig. 5(c)] while the threshold magnitude greater than 100 mV (not presented here) will lead to zero counts in the cases of small size particles. The linear models with these parameters (in the log–log scale) have relatively small fitting errors (as low as 6.5% in NRMSE). On the other hand, in a more complicated scenario that incorporates gap-graded granular particles, the AE counts with 20 mV threshold voltage seem to be the optimal solution (with 15% NRMSE), whereas the fitting errors begin to increase when the threshold voltages move upward and are greater than 20 mV. In contrast, the energy-related AE parameters are struggling to estimate the particle diameters.

Future work will involve AE experimental tests with textured surfaces, in order to induce thick zones of particle shearing along the interface sliding direction. This will help intensify AE signals under high compression stress, whereas the interface sliding with the present smooth shaft sleeve favors rubbing of adjacent glass ballotini over particle shearing/collision [21].

IV. Conclusion

This article has described a test setup that is developed to enable AE measurements of samples of granular materials under 1-D compression and subject to low-stress axial interface shearing against a motion-controlled smooth hollow shaft. The particle size [150 μm, 5 mm], the interface sliding speed [–3 mm/s, +3 mm/s], and the applied stress [0 kPa, 135 kPa] are systematically varied and applied to test the acoustic response. The AE data are processed in both the time- and frequency-domain to extract a group of key parameters including AE energy, AE band power, AE counts (with different threshold voltages), AE count rates, mean and median frequencies, and so on. It is found that either the AE counts or their derivatives (i.e., the AE count rates) can be used to identify the start and end moments of a shearing motion, exhibiting notable step changes, which enables automatic extraction of data segments of interest. Thorough analysis of the dependence of the AE response on the compression

stress, the sliding speed, and particle size, show that energy-related AE parameters and AE counts with a proper threshold voltage can well differentiate particle size (it is proven that any values between 20 and 100 mV are feasible, as 20 mV is just beyond the peak magnitude of AE noise signal according to a histogram analysis, while threshold voltages greater than 100 mV will result in zero counts in the case of small sizes of glass ballotini specimens). Given these facts, linear correlations between these selected AE parameters and the particle diameters are modeled (in log–log scale), facilitating the estimation of the particle size. Moreover, to normalize the scales and ranges of the fitting errors of linear models with different AE parameter, an NRMSE is introduced to enable comparison and assessment of model quality. It shows these linear correlation models are with limited estimation errors (as small as 6.5% in NRMSE) when probing the diameter of a single size of glass ballotini specimen.

The broader applicability of using these correlations to identify a characteristic diameter for a sample is explored by applying the AE method to gap-graded materials (mixtures of coarse and finer granular particles). The presence of different sizes of glass ballotini significantly attenuates the AE signal intensity as compared to the AE response to the single size specimens, making their energy-related linear correlation models not collapsed into the same curve. Despite these complexities, the AE counts at 20 mV threshold voltage can still present two linear correlation models that are relatively close to each other, with 15% fitting errors in NRMSE.

Overall the low stress-varied axial interface shearing induced AE has rich information, which can be used to estimate particle size of granular materials. This technique is particularly suited to in-field geotechnical applications such as in cone penetration testers [14], [24] and new in-site investigation tools of bio-inspired burrowing robots [31], where a steel rod with a conical tip (3.6–4.4 cm in the diameter) is commonly adopted as the framework structure of a instrumentation set-up and moving into the soil from low-stress (near ground) to high-stress area (deeper underground) at a controlled speed (1.5–2.5 cm/s in the case of cone penetration testing while much slower for burrowing robots). Moreover, before applying this technique in the field, additional calibration (using the in-site prototype and the actual soil) is required to account for this scaling effect. This is because, for example, the number of the AE counts are also dependent on the collision volume, as determined by the size of the probe and the number of surrounding soil particles.

REFERENCES

[1] A. Akay, "Acoustics of friction," *J. Acoust. Soc. Amer.*, vol. 111, no. 4, pp. 1525–1548, 2002, doi: 10.1121/1.1456514.

[2] K. Mehraby, H. K. Beheshti, and M. Poursina, "Impact noise radiated by collision of two spheres: Comparison between numerical simulations, experiments and analytical results," *J. Mech. Sci. Technol.*, vol. 25, no. 7, p. 1675, 2011, doi: 10.1007/s12206-011-0503-z.

[3] L. L. Koss and R. J. Alfredson, "Transient sound radiated by spheres undergoing an elastic collision," *J. Sound Vib.*, vol. 27, no. 1, pp. 59–75, Mar. 1973, doi: 10.1016/0022-460X(73)90035-7.

[4] Z. Geng, D. Puhan, and T. Reddyhoff, "Using acoustic emission to characterize friction and wear in dry sliding steel contacts," *Tribol. Int.*, vol. 134, pp. 394–407, Jun. 2019, doi: 10.1016/J.TRIBOINT.2019.02.014.

[5] K. Asamene and M. Sundaresan, "Analysis of experimentally generated friction related acoustic emission signals," *Wear*, vol. 296, nos. 1–2, pp. 607–618, Aug. 2012, doi: 10.1016/J.WEAR.2012.07.019.

[6] J. Ma, H. Zhang, Z. Shi, F. Chu, F. Gu, and A. D. Ball, "Modelling acoustic emissions induced by dynamic fluid-asperity shearing in hydrodynamic lubrication regime," *Tribol. Int.*, vol. 153, Jan. 2021, Art. no. 106590, doi: 10.1016/J.TRIBOINT.2020.106590.

[7] K. Lontin and M. Khan, "Interdependence of friction, wear, and noise: A review," *Friction*, vol. 9, no. 6, pp. 1319–1345, Dec. 2021, doi: 10.1007/S40544-021-0500-X.

[8] H. S. Benabdallah and D. A. Aguilar, "Acoustic emission and its relationship with friction and wear for sliding contact," *Tribol. Trans.*, vol. 51, no. 6, pp. 738–747, Sep. 2008, doi: 10.1080/10402000802044324.

[9] B. Rouet-Leduc, C. Hulbert, N. Lubbers, K. Barros, C. J. Humphreys, and P. A. Johnson, "Machine learning predicts laboratory earthquakes," *Geophys. Res. Lett.*, vol. 44, no. 18, pp. 9276–9282, 2017, doi: 10.1002/2017GL074677.

[10] K. Nakano, "Two dimensionless parameters controlling the occurrence of stick-slip motion in a 1-DOF system with Coulomb friction," *Tribol. Lett.*, vol. 24, no. 2, pp. 91–98, Nov. 2006, doi: 10.1007/s11249-006-9107-7.

[11] F. Avanzini, S. Serafin, and D. Rocchesso, "Interactive simulation of rigid body interaction with friction-induced sound generation," *IEEE Trans. Speech Audio Process.*, vol. 13, no. 5, pp. 1073–1081, Sep. 2005, doi: 10.1109/TSA.2005.852984.

[12] D. Lockner, "The role of acoustic emission in the study of rock fracture," *Int. J. Rock Mech. Mining Sci. Geomech. Abstr.*, vol. 30, no. 7, pp. 883–899, Dec. 1993, doi: 10.1016/0148-9062(93)90041-B.

[13] W. Mao, S. Aoyama, and I. Towhata, "A study on particle breakage behavior during pile penetration process using acoustic emission source location," *Geosci. Frontiers*, vol. 11, no. 2, pp. 413–427, Mar. 2020, doi: 10.1016/J.GSF.2019.04.006.

[14] M. Naderi-Boldaji, M. Z. Tekeste, R. A. Nordstorm, D. J. Barnard, and S. J. Birrell, "A mechanical-dielectric-high frequency acoustic sensor fusion for soil physical characterization," *Comput. Electron. Agricult.*, vol. 156, pp. 10–23, Jan. 2019, doi: 10.1016/J.COMPAG.2018.11.006.

[15] N. K. Wijewardane, S. Hetrick, J. Ackerson, C. L. S. Morgan, and Y. Ge, "VisNIR integrated multi-sensing penetrometer for *in situ* high-resolution vertical soil sensing," *Soil Tillage Res.*, vol. 199, May 2020, Art. no. 104604, doi: 10.1016/J.STILL.2020.104604.

[16] W. Lin, A. Liu, W. Mao, and J. Koseki, "Acoustic emission behavior of granular soils with various ground conditions in drained triaxial compression tests," *Soils Found.*, vol. 60, no. 4, pp. 929–943, Aug. 2020, doi: 10.1016/J.SANDF.2020.06.002.

[17] M. Naderi-Boldaji, M. Bahrami, T. Keller, and D. Or, "Characteristics of acoustic emissions from soil subjected to confined uniaxial compression," *Vadose Zo. J.*, vol. 16, no. 7, pp. 1–12, 2017, doi: 10.2136/vzj2017.02.0049.

[18] P. A. Johnson *et al.*, "Acoustic emission and microslip precursors to stick-slip failure in sheared granular material," *Geophys. Res. Lett.*, vol. 40, no. 21, pp. 5627–5631, Nov. 2013, doi: 10.1002/2013GL057848.

[19] T. A. Brzinski and K. E. Daniels, "Sounds of failure: Passive acoustic measurements of excited vibrational modes," *Phys. Rev. Lett.*, vol. 120, no. 21, May 2018, Art. no. 218003, doi: 10.1103/PhysRevLett.120.218003.

[20] K. Gao, R. Guyer, E. Rougier, C. X. Ren, and P. A. Johnson, "From stress chains to acoustic emission," *Phys. Rev. Lett.*, vol. 123, no. 4, Jul. 2019, Art. no. 48003, doi: 10.1103/PhysRevLett.123.048003.

[21] A. L. Patterson, "The Scherrer formula for X-ray particle size determination," *Phys. Rev. J. Arch.*, vol. 56, pp. 978–982, Nov. 1939, doi: 10.1103/PhysRev.56.978.

[22] R. L. Folk and W. C. Ward, "Brazos river bar [Texas]; a study in the significance of grain size parameters," *J. Sedimentary Res.*, vol. 27, no. 1, pp. 3–26, Mar. 1957, doi: 10.1306/74D70646-2B21-11D7-8648000102C1865D.

[23] T. A. Kettler, J. W. Doran, and T. L. Gilbert, "Simplified method for soil particle-size determination to accompany soil-quality analyses," *Soil Sci. Soc. Amer. J.*, vol. 65, no. 3, pp. 849–852, May 2001, doi: 10.2136/sssaj2001.653849x.

[24] G. L. Hebeler, A. Martinez, and J. D. Frost, "Interface response-based soil classification framework," *Can. Geotech. J.*, vol. 55, no. 12, pp. 1795–1811, Dec. 2018, doi: 10.1139/cgj-2017-0498.

[25] A. Martinez, J. Frost, and G. L. Hebeler, "Experimental study of shear zones formed at sand/steel interfaces in axial and torsional axisymmetric tests," *Geotech. Test. J.*, vol. 38, no. 4, pp. 409–426, 2015, doi: 10.1520/GTJ20140266.
[26] A. Martinez and J. D. Frost, "The influence of surface roughness form on the strength of sand–structure interfaces," *Géotechnique Lett.*, vol. 7, no. 1, pp. 104–111, Mar. 2017, doi: 10.1680/JGELE.16.00169.
[27] A. Martinez and J. D. Frost, "Particle-scale effects on global axial and torsional interface shear behavior," *Int. J. Numer. Anal. Methods Geomech.*, vol. 41, no. 3, pp. 400–421, Feb. 2017, doi: 10.1002/nag.2564.
[28] Y. Hu, L. Wang, X. Huang, X. Qian, L. Gao, and Y. Yan, "On-line sizing of pneumatically conveyed particles through acoustic emission detection and signal analysis," *IEEE Trans. Instrum. Meas.*, vol. 64, no. 5, pp. 1100–1109, May 2015, doi: 10.1109/TIM.2014.2355653.
[29] G. Zheng, Y. Yan, Y. Hu, W. Zhang, L. Yang, and L. Li, "Mass-flow-rate measurement of pneumatically conveyed particles through acoustic emission detection and electrostatic sensing," *IEEE Trans. Instrum. Meas.*, vol. 70, pp. 1–13, 2021, doi: 10.1109/TIM.2020.3039619.
[30] G. Zheng, Y. Yan, Y. Hu, and W. Zhang, "Online measurement of the size distribution of pneumatically conveyed particles through acoustic emission detection and triboelectric sensing," *IEEE Trans. Instrum. Meas.*, vol. 70, pp. 1–17, 2021, doi: 10.1109/TIM.2021.3062407.
[31] N. D. Naclerio *et al.*, "Controlling subterranean forces enables a fast, steerable, burrowing soft robot," *Sci. Robot.*, vol. 6, no. 55, Jun. 2021, Art. no. eabe2922, doi: 10.1126/scirobotics.abe2922.
[32] *Mistras PICO, 200–750 kHz Lightweight Miniature AE Sensor With Integral Coaxial Cable*. Accessed: 2021. [Online]. Available: https://www.physicalacoustics.com/by-product/sensors/PICO-200-750-kHz-Lightweight-Miniature-AE-Sensor-with-Integral-Coaxial-Cable
[33] *Mistras 2/4/6 Switch Selectable Gain Single Ended and Differential Preamplifier*. Accessed: 2020. [Online]. Available: https://www.physicalacoustics.com/by-product/2-4-6/
[34] *Mistras PCI-2 PCI-Based Two-Channel AE Board & System*. Accessed: 2020. [Online]. Available: https://www.physicalacoustics.com/by-product/pci-2/
[35] M. Yu, T. Reddyhoff, D. Dini, A. Holmes, and C. O'Sullivan, "Using ultrasonic reflection resonance to probe stress wave velocity in assemblies of spherical particles," *IEEE Sensors J.*, vol. 21, no. 20, pp. 22489–22498, Oct. 2021, doi: 10.1109/JSEN.2021.3106806.
[36] *Universal Mechanical Tester (UMT)*. Accessed: 2019. [Online]. Available: https://www.bruker.com/en/products-and-solutions/test-and-measurement/tribometers-and-mechanical-testers/umt-tribolab.html
[37] M. Otsubo, R. Kuwano, C. O'Sullivan, and T. Shire, "Using geophysical data to quantify stress transmission in gap-graded granular materials," *Géotechnique*, pp. 1–18, Feb. 2021, doi: 10.1680/jgeot.19.P.334.

Min Yu (Member, IEEE) received the B.Eng. degree in mechanical engineering from Xi'an Jiaotong University, Xi'an, China, in 2011, the M.Sc. degree in mechatronic control engineering from Zhejiang University, Hangzhou, China, in 2014, and the Ph.D. degree in control engineering from Imperial College London, London, U.K., in 2018.

He is currently a Research Associate with the Department of Mechanical Engineering, Imperial College London. His research interests include mechatronics and robotics, dynamics and control, non-destructive sensing, lubrication condition monitoring, and efficiency improvement.

Tom Reddyhoff received the M.Eng. and Ph.D. degrees in mechanical engineering from The University of Sheffield, Sheffield, U.K., in 2003 and 2006, respectively.

He is currently a Reader with the Department of Mechanical Engineering and a member of the Tribology Group. His background is as a mechanical engineer, though the scope of his research has broadened to include the chemistry and physics of surfaces. He has specialized in developing a range of experimental methods, which he uses in combination with numerical modeling to analyze sliding interfaces.

Dr. Reddyhoff holds a five year Engineering and Physical Sciences Research Council (EPSRC) Career Acceleration Fellowship. He has received the Tribology Trust Bronze Medal, a Tiaho Young Tribologist Award and two best paper awards.

Daniele Dini received the master's degree in mechanical engineering from the Politecnico di Bari, Bari, Italy, in 2000, and the D.Phil. degree in engineering science from the University of Oxford, Oxford, U.K., in 2004.

He joined the Department of Mechanical Engineering, Imperial College London, London, U.K., in 2006, where he is currently a Professor in tribology and Head of the Tribology Group. He is also is a Chartered Engineer. His research focuses on the fundamental understanding of the behavior of surfaces and interfaces across the scales and application of advanced modeling techniques to a range of industrial applications.

Prof. Dini is a fellow of the Institution of Mechanical Engineers (IMechE), the Institute of Physics (IoP), and the Society of Tribologists and Lubrication Engineers (STLE), and a member of a number of editorial boards of international journals and committees.

Andrew Holmes (Member, IEEE) received the B.A. degree in natural sciences from Cambridge University, Cambridge, U.K., in 1987, and the Ph.D. degree in electrical engineering from Imperial College London, London, U.K., in 1992.

He is currently a Professor of micro-electro-mechanical systems (MEMS) with the Department of Electrical and Electronic Engineering, Imperial College London. His research interests include micro-power generation by energy harvesting, power conditioning for energy harvesters, tribology of micro-scale mechanical systems, novel micro-assembly techniques, and laser processing for MEMS and electronics manufacture.

Catherine O'Sullivan received the Ph.D. degree with the University of California at Berkeley, Berkeley, CA, USA, in 2002.

She has been a Professor with the Geotechnics Section, Department of Civil and Environmental Engineering, Imperial College London, London, U.K., since September 2017. In 2004, she joined the Department of Civil and Environmental Engineering, Imperial College London, as a Lecturer, following a two-year period at University College Dublin, Dublin, Ireland. Her main research interest is in particulate soil mechanics. Her research uses discrete element modeling (DEM) as well as experimental techniques including micro-computed tomography (μCT). She has been applying these techniques to look at fundamental sand behavior, behavior of reservoir sandstones, internal erosion, and interpretation of laboratory tests.